environmental and earth sciences proceedings

MDPI

Proceeding Paper

Evaluation of Modelling and Remote Sensing Tools for Improving Air Quality in Surroundings of Open Pit Mines †

Raúl Arasa Agudo [1,*], Óscar Hernández [1], Elisa Etzkorn [1], Milagros Herrera [2], David Fuertes [2], Eliot Llopis [2], Ana Sánchez de la Campa [3], Francisco Alejandro [4] and Emilio Sanjuán [4]

[1] Meteosim, 08028 Barcelona, Spain; ohernandez@meteosim.com (Ó.H.); eetzkorn@meteosim.com (E.E.)
[2] GRASP Earth, 59000 Lille, France; milagros.herrera@grasp-earth.com (M.H.); david.fuertes@grasp-earth.com (D.F.); eliot.llopis@grasp-earth.com (E.L.)
[3] Center for Research in Sustainable Chemistry, University of Huelva, 21007 Huelva, Spain; ana.sanchez@pi.uhu.es
[4] Environmental Area, Atalaya Mining, 21660 Minas de Riotinto, Spain; francisco.alejandro@atalayamining.com (F.A.); emilio.sanjuan@atalayamining.com (E.S.)
* Correspondence: rarasa@meteosim.com
† Presented at the 7th International Electronic Conference on Atmospheric Sciences (4–6 June 2025).

Abstract

In this contribution, three techniques related to modelling and remote sensing were tested to answer questions and satisfy requirements from air quality managers in the mining sector: (1) What are appropriate emission factors for blasting operations in copper mines? (2) How can we know the concentration of particulate matter in the next few hours in advance? (3) How can we generate a heat map of the particulate matter levels over the mine and nearby populations? These techniques were evaluated for one of the most relevant open pit mines in southern Europe, the Riotinto Mine, Huelva (Spain). The results obtained suggest that these techniques can efficiently improve the management of air quality in mining activities.

Keywords: particulate matter; mining; modelling; satellite; air quality

Academic Editor: Antonio Donateo

Published: 15 September 2025

Citation: Agudo, R.A.; Hernández, Ó.; Etzkorn, E.; Herrera, M.; Fuertes, D.; Llopis, E.; Sánchez de la Campa, A.; Alejandro, F.; Sanjuán, E. Evaluation of Modelling and Remote Sensing Tools for Improving Air Quality in Surroundings of Open Pit Mines. *Environ. Earth Sci. Proc.* **2025**, *34*, 7. https://doi.org/10.3390/eesp2025034007

1. Introduction

The nature of the activities carried out in an open pit mine requires appropriate and efficient management of the dispersion of pollutants generated and of the local air quality levels [1,2]. The blasting, excavation, and transportation of minerals are some of the main mining activities that can generate the release of particles into the atmosphere [3,4]. These particles may contain heavy metals and other chemical species that can have effects on the respiratory health of people living near mines [5–7].

In this research, three techniques related to air quality modelling and remote sensing were evaluated. These techniques can be qualified as innovative from the point of view that they are not commonly used for the management of air quality in the mining sector, not from a research perspective. These three techniques aim to respond unsolved questions regarding sources of uncertainty identified based on the authors' experiences. Firstly, we evaluated how to calculate the emission factors of blasting activity for copper mines because no recommended values exist for these kinds of mines in the most-used databases, like AP-42 from the US Environmental Protection Agency [8] and EMEP/EEA based on the European Environment Agency's [9] guidelines (the recommended values in these guidelines are representatives for blasting in coal mines). Secondly, a nowcasting tool was

created considering the direct relationship between the concentration of particulate matter and meteorological conditions, like the planetary boundary layer height [10]. And finally, we tested how to generate a heat map of the particulate matter levels over the mine and nearby populations using non-traditional data such as measurement monitoring points.

To address these topics, we tested three techniques: (a) A semi-empirical approach based on the methodology of inverse modelling was used to properly estimate the emission factors of particulate matter released to the atmosphere related to blasting activity. (b) A data-driven model was trained to generate nowcasting results for the levels of particulate matter considering, mainly, the evolution of the meteorological conditions and a high amount of historical concentration data. And (c) an air quality monitoring service that derives particulate matter properties from space by transforming public satellite data and other public sources was tested.

In the scientific literature, there exist many examples of inverse modelling as a technique to estimate the emissions that affect the pollutant concentration [11,12] and of using data-driven models [13,14] and satellite information [15,16] to forecast and diagnose, respectively, the local air quality. But there are not a lot of applications of these techniques to open pit mine environments. The three techniques were evaluated over the Riotinto Mine, Huelva (Spain). Proyecto Riotinto of Atalaya Mining in Minas de Riotinto is the flagship operating mine, a fully operational and conventional open pit. Currently, it comprises two ore deposits: Cerro Colorado and San Dionisio. The site also houses copper concentrate ore processing facilities (15 Mt/year). Copper is an essential component to producing, distributing, and storing renewable energy, and its demand is rising sharply as the world transitions to a low-carbon economy [17].

In the next sections, we present the methodology used (Section 2), the main results obtained (Section 3), and the main findings and conclusions achieved (Section 4).

2. Methods

Summaries regarding every methodology used for every technique analyzed are presented in the next subsections.

2.1. Improvements in Blasting Contribution

The inverse modelling methodology consists of inferences from the Gaussian puff model equation [18] for the mass of PM_{10} emitted in each blast, considering the PM_{10} peak recorded by a sensor that receives the impact of the plume generated for this activity. In doing so, this procedure, with a history of blasts impacting air quality sensors, calculates specific emission factors by relating the emitted mass data to the blast area.

To carry out the inverse modelling, we used the Gaussian puff model equation following the methodology of [19], which considers the evolution of the concentration associated with a plume caused by an instantaneous emission under a uniform wind field. The WRF [20] model at 1 km resolution was used to simulate the wind field and other meteorological variables such as the Pasquill dispersion category, which is necessary to compute some parameters in the methodology of [19].

Pollutant dispersion is very sensitive to the meteorological conditions. For this reason, the WRF model was previously calibrated to the application of the inverse modelling following the methodology of [21], considering the period compressed between July 2021 and June 2024. For this, measurement information from the nearest local meteorological station of El Campillo/El Zumajo, managed by the Spanish National Meteorological Agency (AEMET), was used (37.67° N, 6.59° W, 340 m.a.s.l). A numerical deterministic comparison between the observed and modelled values during this period shows that the MB and RMSE for wind speed are 1.2 m/s and 2.0 m/s, respectively, and a MAGE of 38° was observed

for wind direction. The results obtained indicate that the WRF model provides a reasonable representation of the atmospheric flow conditions relevant for pollutant transport and dispersion.

The inverse modelling methodology was applied to a set of 143 blasts from the period of January 2022 to April 2025 at the Riotinto Mine, for which we had information on the area, time, and coordinates where blasting activity occurred. These 143 blasting episodes were filtered considering those that impact the receptor directly, for which there was no precipitation during the event and natural dust intrusion episodes were discarded.

To estimate the PM_{10} contribution from concentration peaks, 5 min resolution data from a receptor sensor located in the town of La Dehesa (Huelva, Spain; latitude: 37.7137° N; longitude: 6.5822° W), close to the blasting area, were used. All blasting operations for which the wind direction did not favour a perceptible impact on the location of the sensor were discarded.

2.2. Nowcasting of PM_{10} Levels

To forecast the next hourly PM values, a Temporal Fusion Transformer (TFT) was used. The TFT was first introduced in [22] and has been tested and implemented many times, as detailed in the referenced articles [23–26], all of which produced high-quality results. Specifically, the TFT implementation used for the Riotinto case was developed originally by PyTorch Forecasting [27] version 1.3.0. The model has a transformer architecture comprising an LSTM encoder and decoder. This is preceded by input embeddings and followed by variable selection networks and GRNs (gated residual networks). The model also incorporates a multi-head attention mechanism to integrate information across time steps and capture long-term dependencies.

The methodology has been applied over the municipality of Nerva (Huelva, Spain); (latitude: 37.6952° N; longitude: 6.5507° W). This receptor point is located relatively far from the mine and is therefore less influenced by uncontrolled direct emissions, which can generate instant peaks of particulate matter that are very difficult to reproduce. However, it is still influenced by the mine's overall activity.

The data used to train the model comes from two different sources: the particulate matter concentration, measured in monitoring points, such as other meteorological variables measured by the mine's sensors, and the hourly forecast obtained using GFS [28] and WRF models. Several meteorological variables from meteorological forecasts were included for their influence on the concentration of particulate matter. Further details about the features can be found in Table 1, and the hyperparameters are specified in Table A1 in Appendix A. The training period selected was two years and began in June 2021. The testing period ran until the end of 2023.

Table 1. Names of the features used to train the TFT.

Features	
Target values	PM_{10}, $PM_{2.5}$
Known real values	Hour, weekday, week, month, forecasted meteorological variables
Unknown real values	Measured meteorological variables
Categorical values	None
Static values	None

2.3. Elaboration of Heat Maps Using Satellite Data

The third technique evaluated in this study involves generating high-resolution heat maps of particulate matter concentrations in and around the Riotinto Mine using different

remote sensing instruments. For this purpose, in our study, we used the satellite-based air quality monitoring tool based on the GRASP algorithm (Generalized Retrieval of Atmosphere and Surface Properties). GRASP is one of the most advanced algorithms for aerosol and surface properties determined using different instruments, and it was selected for upcoming public space missions such as Sentinel-4, Sentinel-7, and 3 MI due to its proven performance [29–31].

The GRASP algorithm takes as input different satellite data to provide spatially detailed estimations of $PM_{2.5}$ and PM_{10} levels and different aerosol products. The resolution of the products is relayed to the resolution of the satellite data; in this case, the PM_{10} and $PM_{2.5}$ satellite-derived products were based on OLCI (S3—300 m–500 m resolution), TROPOMI (S5P—7 × 3 km), and PARASOL (POLDER—6 km) data.

3. Results and Discussion

3.1. Improvements in Blasting Contributions

Out of the 143 recorded blasts analyzed, there were only 2 that satisfied the conditions defined to infer the emission by the inverse modelling methodology.

Figure 1 shows the PM_{10} concentration field caused by one of the analyzed blasting operations, on 12 March 2025, with a blasted area of 1800 m^2, simulated with a Gaussian plume model. It corresponds to an illustrative comparison between the simulation using the mass emitted according to the emission factors established in the AP-42 on the left and that using the mass emitted inferred by inverse modelling from the peak recorded at the La Dehesa receptor on the right, from which the contribution of the blasting to the PM_{10} concentration was estimated to be 104 $\mu g/m^3$. In this case, with a southwest (SW) wind, the mass emitted estimated by the AP-42 emission factor was 6.63 kg, whereas via inverse modelling, it was 1.40 kg. The emissions estimated using the inverse modelling method are almost five times lower than those obtained using the standard AP-42 emission factor. This is because, as we indicated previously, the standard AP-42 emission factor is valid for coal mines, and coal's pulverizing capacity is greater than that of copper, given its lower density, hardness, and moisture content. Table 2 shows the emissions considered, the concentration estimated by modelling, and the estimated contribution of the blasting to the PM_{10} concentration.

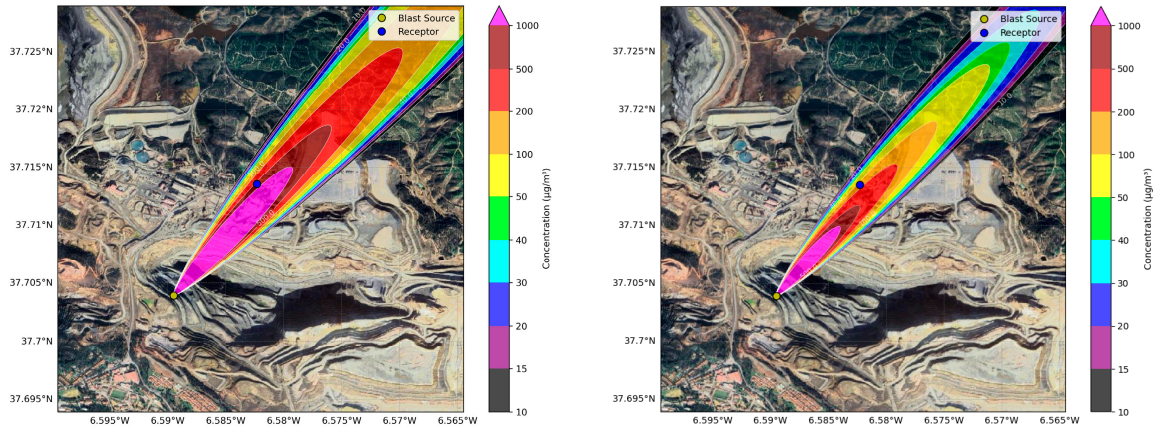

Figure 1. Comparison of the PM_{10} concentration obtained using Gaussian dispersion modelling and emissions calculated by AP-42 emission factors (**left**) and estimated using inverse modelling (**right**).

Table 2. Comparison between the modelled concentration using different emission factor estimations and the estimated contribution of the blasting to the PM_{10} concentration for the episode of 12 March 2025.

Emission Factor Estimation Method	Emission	Modelled Concentration	Estimated Contribution of the Blasting to PM_{10} Concentration	Difference Between Modelled and Observed
AP-42	6.63 kg	651 µg/m^3	104 µg/m^3	547 µg/m^3 (526%)
Inverse Modelling	1.40 kg	137 µg/m^3		33 µg/m^3 (32%)

3.2. Nowcasting of PM_{10} Levels

Overall, the trained TFT model achieves mean absolute errors (MAEs) of 3.0 µg/m^3 and 1.6 µg/m^3 for PM_{10} and $PM_{2.5}$, respectively.

In Figure 2 (above), the r^2 score is presented for both pollutants and compared to the persistence performance, following the recommendations of [32], where persistence means the order 0 forecast, i.e., the last observed value. The difference between the TFT and persistence grows larger with each forecasted hour and is more notable in PM_{10}, which is consistent with this pollutant's higher variability due to its greater number of possible emission sources. Furthermore, since persistence loses value over time, it is expected that the TFT will display better performance when increasing the forecasted hour. On the other hand, despite displaying an expected behaviour, the r^2 values are low, possibly indicating a missing PM source in our training dataset, most probably data related to the mine's activity.

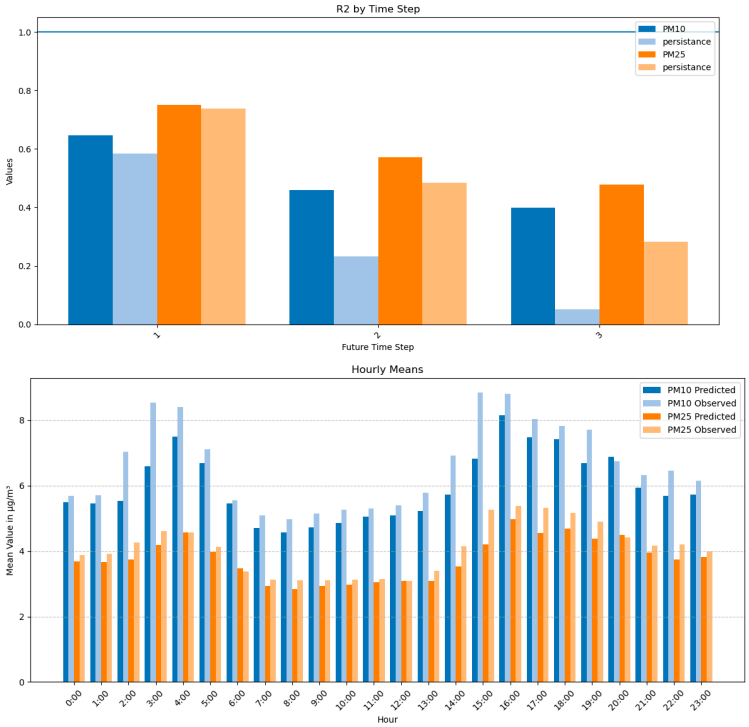

Figure 2. r^2 score for PM_{10} and $PM_{2.5}$ compared with the persistence forecast (**above**) and a comparison of the mean hourly values forecasted and observed throughout the day (**below**).

Finally, Figure 2 (below) shows the mean hourly values of the forecasts and of the observed values throughout the day. The observed and forecasted means are very similar, and the means of the TFT forecast correctly follow the observed mean profile. Nevertheless, the model consistently predicts lower values than the actual measurements. This is because the model struggles to predict sudden increases in the data, or peaks, which show no clear patterns as they are influenced by mining activity, which was not included in the training.

Other aspects that may impact model performance and explain the low r^2 values and this systematic underestimation are systematic errors in the WRF-modelled wind direction caused by the higher topographical variability around the mine site.

3.3. Elaboration of Heat Maps Using Satellite Data

The use of the GRASP algorithm with satellite remote sensing data for monitoring particulate matter concentrations has demonstrated valuable potential, particularly at higher resolutions. Figure 3 shows the PM_{10} concentration levels over the Riotinto Mine area using Sentinel-3/OLCI observations on 6 and 20 July 2019. Retrievals were processed using the GRASP/OLCI algorithm, which incorporates a priori constraints based on ancillary datasets such as VIIRS and POLDER to improve the accuracy of the aerosol characterization.

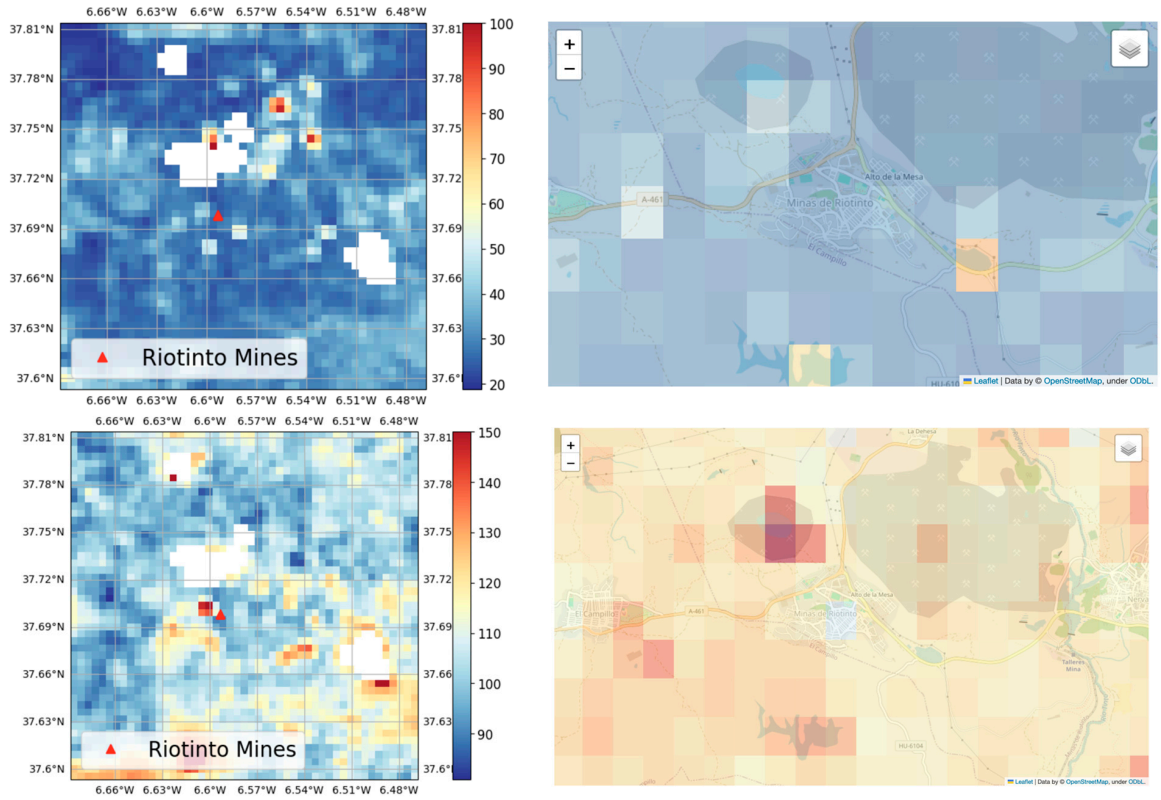

Figure 3. Spatial variability in PM_{10} ($\mu g/m^3$) at the Riotinto Mine and its surroundings determined using GRASP/OLCI methodology for 6 July (**above**) and 20 July(**below**), 2019 (**left**). Zoom of this spatial variability near Riotinto mine (**right**).

The PM_{10} heat map, shown in the left panel, illustrates spatial variability with concentrations around the Riotinto Mine. The map on the right shows a zoomed-in area for the same data over the Riotinto Mines. One key advantage of the GRASP/OLCI methodology is its spatial resolution—300 m—which is sufficient for detecting more details around the Riotinto Mine and surrounding areas. This level of detail is particularly suited for applications involving environmental management and exposure assessment in industrial regions.

4. Conclusions

Three technologies were tested with the aim of improving the management of air quality in an open pit mine and its surroundings. The main conclusions achieved through this research include the following:

(1) As standard emissions factors for blasting operations like AP-42 are based on coal mines, they do not correctly apply to copper mines, generating a relevant overestimation of the concentration generated by blasts. The inverse modelling methodology is a simple, useful, effective, and scalable tool for calculating emission factors that are more appropriate than those of the standards.
(2) The nowcasting technique enables us to determine, with a high degree of accuracy, the evolution of this pollutant over the next few hours (1, 2, 3 h). The TFT model developed adds value compared to persistence forecasting, showing low levels of MAEs, 3.0 $\mu g/m^3$ and 1.6 $\mu g/m^3$ for PM_{10} and $PM_{2.5}$, respectively, indicating reliable performance in predicting these pollutants.
(3) GRASP satellite observations provide a powerful tool for hindcast analysis, long-term trend evaluation, and spatial hotspot detection, providing essential input for risk assessment and targeted air quality interventions. These capabilities are crucial for understanding the environmental footprint of mining operations and for informing public health strategies in affected areas.

Some areas of limitations and improvement are identified for this research work. Thus, the following activities are considered for future work:

- For the blasting contributions, only two episodes were identified that meet all defined conditions. It is necessary to expand the analysis for a longer period. Furthermore, the inverse modelling estimation can be extended considering the type of material (mineral or sterile), pollutants, $PM_{2.5}$, and heavy metals. Also, incorporating CFD (Computational Fluid Dynamics) modelling can help us obtain a better representation of the pollutant dispersion.
- In the case of the nowcasting study, PM_{10} shows lower accuracy in comparison with $PM_{2.5}$ due to higher emission source contributions and higher uncertainty in measurements, as well as higher difficulty in representing exceedances of the legislated limit values. For this reason, the use of a more representative period is required to validate nowcasting results and focus on exceedance forecasts.
- Finally, in the case of the hindcast analysis, a limitation remains regarding the revisit frequency of Sentinel-3 that it is currently limited to once every 2–3 days. Incorporating future satellite missions with a higher revisit frequency will improve the possibilities of hindcast analysis. Also, coupling surface information from monitoring points with satellite information can improve the heat maps generated.

Author Contributions: Conceptualization, R.A.A.; methodology, R.A.A., Ó.H., E.E., M.H. and D.F.; software, Ó.H., E.E. and M.H.; validation, Ó.H., E.E. and M.H.; formal analysis, R.A.A., Ó.H., E.E. and M.H.; investigation, R.A.A., Ó.H., E.E. and M.H.; resources, F.A. and M.H.; data curation, F.A. and M.H.; writing—original draft preparation, R.A.A., Ó.H., E.E., M.H. and F.A.; writing—review and editing, R.A.A. and A.S.d.l.C.; visualization, Ó.H., E.E. and M.H.; supervision, R.A.A., D.F., A.S.d.l.C., F.A., E.L. and E.S.; project administration, R.A.A.; funding acquisition, D.F. All authors have read and agreed to the published version of the manuscript.

Funding: The research associated with the satellite data was funded by the European Space Agency (ESA) under Contract No. 4000145377/24/NL/GM/jxh. The other tasks received no external funding.

Data Availability Statement: The datasets presented in this article are not readily available because they are part of an ongoing study.

Acknowledgments: The authors would like to kindly thank Jesús D. de la Rosa of CIQSO/UHU for providing the data from the air quality stations used and for his collaboration in the conception and design of the research, as well as Atalaya Mining for participating in the research study and facilitating access to the information required for the study.

Conflicts of Interest: The authors declare no conflicts of interest.

Abbreviations

The following abbreviations are used in this manuscript:

AEMET	Spanish National Meteorological Agency;
CFD	Computational Fluid Dynamics;
CIQSO	Center for Research in Sustainable Chemistry;
GFS	Global Forecasting System;
GRASP	Generalized Retrieval of Atmosphere and Surface Properties;
GRN	Gated Residual Network;
MAGE	Mean Absolute Gross Error;
MB	Mean Bias;
RMSE	Root Mean Square Error;
TFT	Temporal Fusion Transformer;
UHU	University of Huelva;
WRF	Weather Research and Forecasting System.

Appendix A

Table A1. Hyperparameters used for the TFT model.

Hyperparameters		
Epochs	200	No. of iterations over the data
Prediction length	3	No. of future time steps
Encoder length	48	No. of past time steps in the input
Learning rate	0.068	Step size for model optimization
Batch size	32	No. of training samples in a single pass
Dropout	0.1	Fraction of dropped neurons
Loss function	Quantile loss	--
Attention head size	1	No. of parallel attention heads
Hidden size	8	Dimensions of the model's layers

References

1. Boente, C.; Zafra-Pérez, A.; Fernández-Caliani, J.C.; Sánchez de la Campa, A.M.; Sánchez-Rodas, D.; de la Rosa, J.D. Source apportionment of potentially toxic PM10 near a vast metallic ore mine and health risk assessment for residents exposed. *Atmos. Environ.* **2023**, *301*, 119696. [CrossRef]
2. Huertas, J.I.; Huertas, M.E.; Izquierdo, S.; González, E.D. Air quality impact assessment of multiple open pit coal mines in northern Colombia. *J. Environ. Manag.* **2012**, *93*, 121–129. [CrossRef]
3. Boente, C.; Millán-Martínez, M.; Sánchez de la Campa, A.M.; Sánchez-Rodas, D.; de la Rosa, J.D. Physicochemical assessment of atmospheric particulate matter emissions during open-pit mining operations in a massive sulphide ore exploitation. *Atmos. Pollut. Res.* **2022**, *13*, 101391. [CrossRef]
4. Petavratzi, E.; Kingman, S.; Lowndes, I. Particulates from mining operations: A review of sources, effects and regulations. *Miner. Eng.* **2005**, *18*, 1183–1199. [CrossRef]
5. Castillo, S.; de la Rosa, J.D.; Sánchez de la Campa, A.M.; González-Castanedo, Y.; Fernández-Caliani, J.C.; Fernández Camacho, R.; González, I.; Romero, A. Contribution of mine wastes to atmospheric metal deposition in the surrounding area o fan abandoned heavily polluted mining district (Riotinto Mines, Spain). *Sci. Total Environ.* **2013**, *449*, 363–372. [CrossRef]
6. Fernández Caliani, J.C.; de la Rosa, J.D.; Sánchez de la Campa, A.M.; González Castanedo, S.; Castillo, S. Mineral composition of atmospheric fallout impacting the Riotinto mining area (Spain) during episodes of high metal deposition. *Mineral. Mag.* **2013**, *77*, 2793–2810. [CrossRef]

7. Sánchez de la Campa, A.M.; de la Rosa, J.D.; Fernández Caliani, J.C.; Gonzalez-Castanedo, Y. Impact of abandoned mine wastes on atmospheric respirable particulate matter in the historic mining district of Riotinto (Iberian Pyrite Belt). *Environ. Res.* **2011**, *111*, 1018–1023. [CrossRef] [PubMed]
8. AP-42: Compilation of Air Emissions Factors from Stationary Sources. Available online: https://www.epa.gov/air-emissions-factors-and-quantification/ap-42-compilation-air-emissions-factors-stationary-sources (accessed on 21 May 2025).
9. EMEP/EEA air pollutant emission inventory guidebook 2023. Available online: https://www.eea.europa.eu/en/analysis/publications/emep-eea-guidebook-2023 (accessed on 21 May 2025).
10. Comas Muguruza, A.; Arasa Agudo, R.; Udina, M. Characterization of the Planetary Boundary Layer Height in Huelva (Spain) During an Episode of High NO_2 Pollutant Concentrations. *Earth* **2025**, *6*, 26. [CrossRef]
11. Kumar, S.; Sharma, S.; Sharma, P.; Agarwal, S. Inverse modelling approach to assess air pollutant emission trends, and source contributions in highly polluted cities. *Discov. Atmos.* **2024**, *2*, 13. [CrossRef]
12. Cheng, X.; Hao, Z.; Zang, Z.; Liu, Z.; Xu, X.; Wang, S.; Liu, Y.; Hu, Y.; Ma, X. A new inverse modeling approach for emission sources based on the DDM-3D and 3DVAR techniques: An application to air quality forecasts in the Beijing–Tianjin–Hebei region. *Atmos. Chem. Phys.* **2021**, *21*, 13747–13761. [CrossRef]
13. Rosca, C.-M.; Carbureanu, M.; Stancu, A. Data-Driven Approaches for Predicting and Forecasting Air Quality in Urban Areas. *Appl. Sci.* **2025**, *15*, 4390. [CrossRef]
14. Wu, C.; Wang, R.; Lu, S.; Tian, J.; Yin, L.; Wang, L.; Zheng, W. Time-Series Data-Driven $PM_{2.5}$ Forecasting: From Theoretical Framework to Empirical Analysis. *Atmosphere* **2025**, *16*, 292. [CrossRef]
15. Anggraini, T.S.; Irie, H.; Sakti, A.D.; Wikantika, K. Global air quality index prediction using integrated spatial observation data and geographics machine learning. *Sci. Remote Sens.* **2025**, *11*, 100197. [CrossRef]
16. Stebel, K.; Stachlewska, I.S.; Nemuc, A.; Horálek, J.; Schneider, P.; Ajtai, N.; Diamandi, A.; Benešová, N.; Boldeanu, M.; Botezan, C.; et al. SAMIRA-SAtellite Based Monitoring Initiative for Regional Air Quality. *Remote Sens.* **2021**, *13*, 2219. [CrossRef]
17. Seck, G.S.; Hache, E.; Bonnet, C.; Simoën, M.; Carcanague, S. Copper at the crossroads: Assessment of the interactions between low-carbon energy transition and supply limitations. *Resour. Conserv. Recycl.* **2020**, *163*, 105072. [CrossRef]
18. Snoun, H.; Krichen, M.; Chérif, H. A comprehensive review of Gaussian atmospheric dispersion models: Current usage and future perspectives. *Euro-Mediterr. J. Environ. Integr.* **2023**, *8*, 219–242. [CrossRef]
19. Roy, S.; Adhikari, G.R.; Singh, T.N. Development of Emission Factors for Quantification of Blasting Dust at Surface. *J. Environ. Prot.* **2010**, *1*, 346–361. [CrossRef]
20. Skamarock, W.C.; Klemp, J.B.; Dudhia, J.; Gill, D.O.; Barker, D.M.; Duda, M.G.; Huang, X.-Y.; Wang, W.; Powers, J.G. *A Description of the Advanced Research WRF Version 3*; NCAR Technical Note 475; National Center for Atmospheric Research: Boulder, CO, USA, 2008.
21. Arasa, R.; Porras, I.; Domingo-Dalmau, A.; Picanyol, M.; Codina, B.; González, M.; Piñón, J. Defining a Standard Methodology to Obtain Optimum WRF Configuration for Operational Forecast: Application over the Port of Huelva (Southern Spain). *Atmos. Clim. Sci.* **2016**, *6*, 329–350. [CrossRef]
22. Lim, B.; Arık, S.; Loeff, N.; Pfister, T. Temporal fusion transformers for interpretable multi-horizon time series forecasting. *Int. J. Forecast.* **2021**, *37*, 1748–1764. [CrossRef]
23. Badhe, N.; Neve, R.; Yele, V.; Abhang, S.; Dhule, K.; Mali, D. An optimized system for predicting energy usage in smart grids using temporal fusion transformer and aquila optimizer. *Front. Artif. Intell.* **2025**, *8*, 1542320. [CrossRef] [PubMed]
24. Lekidis, A.; Papageorgiou, E. Edge-based short-term energy demand prediction. *Energies* **2023**, *16*, 5435. [CrossRef]
25. Saleem, M.; Rashid, J.; Ahmad, S.; Al-Shaery, A.; Althobaiti, S.; Faheem, M. Forecasting green energy production in latin american countries and Canada via temporal fusion transformer. *Energy Sci. Eng.* **2025**, *13*, 2262–2283. [CrossRef]
26. Yang, H.; Li, P.; Cui, Y.; Han, X.; Zhou, M. Multi-sensor temporal fusion transformer for stock performance prediction: An adaptive sharpe ratio approach. *Sensors* **2025**, *25*, 976. [CrossRef]
27. PyTorch Forecasting—Temporal Fusion Transformer. Available online: https://pytorch-forecasting.readthedocs.io/en/stable/api/pytorch_forecasting.models.temporal_fusion_transformer._tft.TemporalFusionTransformer.html (accessed on 16 January 2025).
28. NOAA The Global Forecasting System (GFS). Available online: https://www.emc.ncep.noaa.gov/emc/pages/numerical_forecast_systems/gfs/documentation.php (accessed on 24 March 2025).
29. Dubovik, O.; Lapyonok, T.; Litvinov, P.; Herman, M.; Fuertes, D.; Ducos, F.; Lopatin, A.; Chaikovsky, A.; Torres, B.; Derimian, Y.; et al. GRASP: A versatile algorithm for characterizing the atmosphere. *SPIE Newsroom* **2014**, *25*, 2–1201408. [CrossRef]
30. Dubovik, O.; Fuertes, D.; Litvinov, P.; Lopatin, A.; Lapyonok, T.; Doubovik, I.; Xu, F.; Ducos, F.; Chen, C.; Torres, B.; et al. A comprehensive description of multi-term LSM for applying multiple a priori constraints in problems of atmospheric remote sensing: GRASP algorithm, concept, and applications. *Front. Remote Sens.* **2021**, *2*, 706851. [CrossRef]

31. Chen, C.; Dubovik, O.; Fuertes, D.; Litvinov, P.; Lapyonok, T.; Lopatin, A.; Ducos, F.; Derimian, Y.; Herman, M.; Tanré, D.; et al. Validation of GRASP algorithm product from POLDER/PARASOL data and assessment of multi-angular polarimetry potential for aerosol monitoring. *Earth Syst. Sci. Data* **2020**, *12*, 3573–3620. [CrossRef]
32. Janssen, S.; Thunis, P. *FAIRMODE Guidance Document on Modelling Quality Objectives and Benchmarking (Version 3.3)*; EUR 31068 EN; JRC129254; Publications Office of the European Union: Luxembourg, 2022; ISBN 978-92-76-52425-0. [CrossRef]